

# Visual Servoing of an Airplane for Auto-Landing

Odile Bourquardez and François Chaumette

**Abstract**—In this paper, a visual servoing scheme is proposed to control an airplane during its landing. A linearized model of the airplane dynamics and decoupled visual features are used to build the control scheme. A desired trajectory which takes into account the airplane dynamic is designed. Coupling this trajectory and the control law enables the airplane to join its desired path. Then the airplane is controlled to follow the glide path, realize the flare manoeuvre and finally touchdown. Simulation results are obtained with a quite realistic flight simulator which is based on a non linear airplane dynamic model. They show that the airplane is able to land automatically by using visual data.

## I. INTRODUCTION

Visual servoing schemes enable to control robot motion by using visual features as feedback signal [4] [7]. The camera can be embedded on the robot or be placed in its external environment. Different kinds of visual features can be used to design the control law: 2D data, directly extracted from the image, or 3D data, provided by a preliminary pose estimation (a mixture of the both can also be used [12]).

Using visual servoing to control aircraft yields new problems. Indeed, in most robotics applications, the degrees of freedom can be assumed to be as a pure integrator leading to kinematics control schemes. But designing visual servoing for aircraft requires to take into account their dynamic constraints.

In a lot of works, the vision sensor is used to provide pose estimation. The control law is then based on the position, and other sensors such as GPS or inertial sensors can be used in the control law. This strategy is used in [14] [17] [18] to control helicopters. In [3] a camera is used with inertial gyros and air velocity meter. Then the data are filtered for estimation of the state vector of an airplane. In this paper, we have chosen to not deal with pose estimation, but to consider 2D visual servoing. The most common 2D approach to control aircraft is to consider state equations and to link the state vector with the visual features. For instance, in [20] the authors incorporate the dynamics of a blimp in the equations of the image dynamics, and apply a PID control. In [1] [15] [16] the state model is linearized around an equilibrium state and the visual features are used as measurement outputs. Then standard control design such as LQR (Linear Quadratic Regulator) can be used with the LTI (Linear Time Invariant) system obtained. We have used a similar approach for the longitudinal control. However,

the proposed lateral control is based on a simple constraint applied to the lateral position.

Several strategies have already been used to follow linear structures by visual servoing. In [11], the binormalized Plücker coordinates of the lines are used, and the dynamic properties of helicopters are exploited to design a control scheme based on a Lyapunov function and backstepping techniques. In [16] vanishing point and vanishing line have been considered in a 2D visual servoing scheme for controlling a blimp. The scheme presented in [19] uses only two lines, and the camera is thus combined with other sensors in order to fully control the state parameters of a blimp. Lateral position of a small autonomous aircraft with respect to a road is performed in [5] by partial 3D pose estimation. In our case, we have designed new decoupled visual features in order to improve the relationship with the aircraft state. In previous work [2], we have considered three parallel lines, which could belong to a road or a runway for example. The aim was to align the airplane with respect to this structure with constant attitude, velocity, and altitude.

Landing is a critical flight task that can be divided into several phases. During the approach the airplane has to follow a glide-path which is a linear trajectory, with constant velocity  $v_a$  and slope  $\gamma$  (see Fig. 1). When the required altitude is reached, the flare manoeuvre is activated, until touch down [3], [8], [9], [10]. During all the phases, the airplane has to stay aligned with the runway axis.

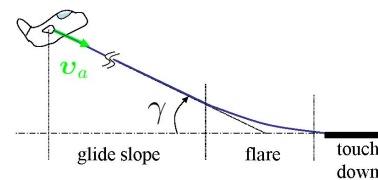


Fig. 1. Landing phases.

In this paper, an airplane equipped with a camera has to join the glide-path, follow it, and realize the flare manoeuvre in order to touchdown. We propose to apply the control schemes of [2] to the auto-landing task. The approach is strongly improved by designing adequate variable trajectories. The airplane is able to join the glide-path from further positions, and its behaviour is smoother. As in [2], an airplane equipped with a fly-by-wire system is considered: the pilot commands are converted to electronic signals, and flight control computers determine how best to move the actuators to provide the desired response.

This paper is organized as follows: in Section II the no-

O. Bourquardez is with IRISA-CNRS, Campus de Beaulieu, 35042 Rennes cedex, France [odile.bourquardez@irisa.fr](mailto:odile.bourquardez@irisa.fr)

F. Chaumette is with IRISA-INRIA, Campus de Beaulieu, 35042 Rennes cedex, France [francois.chaumette@irisa.fr](mailto:francois.chaumette@irisa.fr)

tations are introduced and the relationship between the pilot commands and the airplane motion is given by a linearized model. In Section III trajectories design are proposed to reach the glide-path from any initial position, follow it and round the trajectory in order to realize touchdown in suitable conditions. In Section IV the trajectories are transformed in desired visual features and a visual servoing scheme is used to control the airplane. Simulation results are shown in Section V. Instead of being performed with the linearized model, the simulations use a more complete and realistic flight simulator. They show that the proposed control scheme enables the aircraft to land automatically.

## II. AIRCRAFT MODEL

### A. Control Inputs

In most of previous works, the control inputs are actuators deflection and thrust produced by the propellers. In this paper, the aircraft considered is equipped with a fly-by-wire system: instead of using cables, computer-generated electrical signals are used to transmit the pilot commands to the flight control surfaces. The fly-by-wire system provides additionally safety control to prevent insecure pilot commands. For safety reasons, it is thus preferable to leave unchanged this low-level flight control system and to deal with the pilot commands. Thus the considered inputs to control the aircraft are the throttle position and the control stick.

Let  $\mathbf{u} = (\delta_m, \delta_l, \delta_T)$  denote the input vector.  $\delta_m \in [-1; 1]$  is the control stick forward-backward position, and it mainly controls the angle of attack.  $\delta_l \in [-1; 1]$  is the control stick left-right position, and it mainly induces rotation around the longitudinal axis. Finally  $\delta_T \in [0; 1]$  is the throttle position, and it is related to thrust level. However, due to the aircraft dynamics, these movements are coupled and induce other trajectory or attitude modifications.

### B. State Components and other Notations

Let  $\mathcal{R}_a$  denote the aircraft frame, and  $\mathcal{R}_f$  a fixed reference frame (see Fig. 2). The aircraft pose is defined by the translation and the rotation between  $\mathcal{R}_a$  and  $\mathcal{R}_f$ . Let  $(X, Y, Z)$  denote the three components of the translation, and  $(\phi, \theta, \psi)$  denote the roll-pitch-yaw angles of the rotation. Let  $\mathbf{P} = (X, Y, Z, \phi, \theta, \psi)$  denote the pose vector.

The primary way for a pilot to change the airplane direction is to change the aircraft attitude. Let  $\mathbf{v}_a = (v_{a_x}, v_{a_y}, v_{a_z}, \omega_{a_x}, \omega_{a_y}, \omega_{a_z})$  denote the aircraft instantaneous velocity (see Fig. 2.a), and  $\mathbf{v}_a = (v_{a_x}, v_{a_y}, v_{a_z})$  its translational velocity,  $v_a$  its module, and  $\dot{v}_a$  the module of the acceleration. Note that in most cases the velocity vector  $\mathbf{v}_a$  and the aircraft longitudinal axis  $x_a$  have not the same direction. Let  $\gamma$  denote the slope angle, between the horizontal plane and the velocity vector (see Fig. 2.b).

### C. Linearized Model

The airplane dynamics model which links the pilot inputs and the aircraft motions have been provided by the French company Dassault Aviation. We have first linearized this

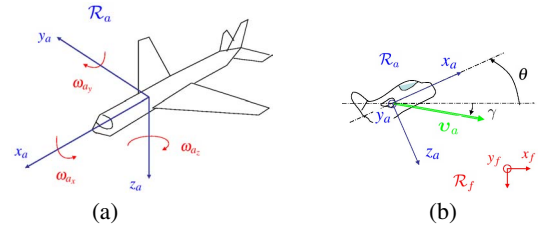


Fig. 2. (a) Aircraft frame and associated rotations, (b) Angles definitions. model to design the control scheme, but the real one has been used to validate the control scheme. For that, the classical hypothesis of small perturbations around a trim flight is considered. We use the following approximation:  $\dot{\mathbf{P}} = \mathbf{v}_a$ . Moreover the angle of side slip has been neglected and  $\phi$  and  $\dot{\psi}$  are supposed to be proportionnal. Considering the motor dynamics leads to introduce  $\dot{v}_a$  in the state.

Finally the aircraft model can be represented by the following state space equation:  $\dot{\mathbf{x}} = \mathbf{A}\mathbf{x} + \mathbf{B}\mathbf{u}$  with  $\mathbf{x} = (\phi, \dot{\psi}, \psi, Y, \theta, \dot{\theta}, \gamma, v_a, \dot{v}_a, Z)$ . This model can be decoupled between the lateral motion in the horizontal plane (1), and the longitudinal motion in the vertical plane (2).  $\tilde{w} = w - w_0$  represents the variation between the current value  $w$  and the equilibrium value  $w_0$  for any  $w$  parameter. (Note that the equilibrium values are null in the lateral model). The constants  $a_1, \dots, a_{19}, b_1, \dots, b_4$  are determined from aircraft constants and state equilibrium values.

$$\begin{bmatrix} \ddot{\phi} \\ \ddot{\psi} \\ \dot{\psi} \\ \dot{Y} \end{bmatrix} = \begin{bmatrix} a_1 & 0 & 0 & 0 \\ a_3 & 0 & 0 & 0 \\ 0 & 1 & 0 & 0 \\ 0 & 0 & a_5 & 0 \end{bmatrix} \begin{bmatrix} \dot{\phi} \\ \dot{\psi} \\ \psi \\ Y \end{bmatrix} + \begin{bmatrix} b_1 \\ 0 \\ 0 \\ 0 \end{bmatrix} \delta_l \quad (1)$$

$$\begin{bmatrix} \ddot{\theta} \\ \ddot{\theta} \\ \ddot{\gamma} \\ \ddot{v}_a \\ \ddot{v}_a \\ \ddot{Z} \end{bmatrix} = \begin{bmatrix} 0 & 1 & 0 & 0 & 0 & 0 \\ a_6 & a_7 & 0 & a_8 & 0 & 0 \\ a_9 & 0 & a_{10} & a_{11} & a_{12} & 0 \\ 0 & 0 & 0 & 0 & 1 & 0 \\ a_{13} & a_{14} & a_{15} & a_{16} & a_{17} & 0 \\ 0 & 0 & a_{18} & a_{19} & 0 & 0 \end{bmatrix} \begin{bmatrix} \dot{\theta} \\ \dot{\theta} \\ \dot{\gamma} \\ \dot{v}_a \\ \dot{v}_a \\ \dot{Z} \end{bmatrix} + \begin{bmatrix} 0 & 0 \\ b_3 & 0 \\ 0 & 0 \\ 0 & 0 \\ 0 & b_4 \\ 0 & 0 \end{bmatrix} \begin{bmatrix} \tilde{\delta}_m \\ \tilde{\delta}_T \end{bmatrix} \quad (2)$$

## III. LANDING PHASES

### A. Joining the glide path

1) *Lateral Motion*: We consider that the airplane has an initial position  $Y_i$  and orientation  $\psi_i$  with respect to the fixed frame attached to the runway (see Fig 3). To join the glide-path the airplane has to align with the runway (so that the lateral position  $Y$  and heading angle  $\psi$  are null).

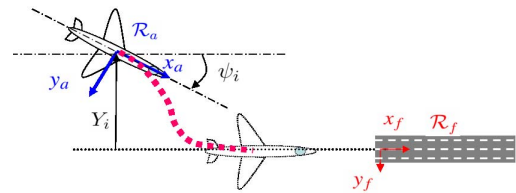


Fig. 3. Lateral initial and final position of the airplane with respect to the runway.

When the initial lateral error is large, using a step as desired position in a visual servoing scheme can lead to an

undesirable behaviour. In that case it is necessary to design a trajectory which takes into account the lateral dynamics of the airplane and to control the aircraft so that it follows this trajectory. The airplane behaviour will then be smooth in reaching the gliding slope.

The problem is to design a function  $Y^*(t)$  that describes the airplane lateral desired position, and enables to reach the desired position  $Y_f = 0$  from an initial position  $Y_i$ . We consider that the trajectory starts at time  $t = t_0$  and finishes at time  $t = t_f$ .

The first essential conditions are to reach the initial and final positions:

$$Y^*(t_0) = Y_i, \quad Y^*(t_f) = 0. \quad (3)$$

Then, to improve the behaviour, we have to consider the initial and final values of the derivative of  $Y^*$ . Using the lateral linear model (1) we can see that

$$\dot{Y} = a_5 \psi, \quad (4)$$

i.e.  $\dot{Y}$  is directly related to the heading angle. Thus the corresponding initial and final conditions deal with the initial and final heading  $\psi_i$  and  $\psi_f = 0$ :

$$\dot{Y}^*(t_0) = a_5 \psi_i, \quad \dot{Y}^*(t_f) = 0. \quad (5)$$

By repeating again this idea, we also constrain the derivative of  $\psi^*$ . The second line of the model (1) yields to the following link between  $\dot{\psi}$  and  $\phi$ :

$$\dot{\psi} = a_3 \phi \quad (6)$$

Then recalling (4) yields

$$\ddot{Y} = a_5 a_3 \phi. \quad (7)$$

Constraining the derivative of  $\psi^*$  corresponds to constrain  $\dot{Y}$  and thus the initial and final roll  $\phi_i$  and  $\phi_f = 0$ :

$$\dot{Y}^*(t_0) = a_5 a_3 \phi_i, \quad \dot{Y}^*(t_f) = 0. \quad (8)$$

Finally, in order to improve the behaviour of the roll angle  $\phi_i$ , we now consider its derivative  $\dot{\phi}_i$ , and constrain it to be null at the start and at the end. Using the first line of (1), assuming that  $\delta_l$  is constant and integrating the differential equation  $\ddot{\phi}(t) = a_1 \dot{\phi}(t) + b_1 \delta_l$  gives

$$\dot{\phi} = c_1 e^{a_1 t} - \frac{b_1}{a_1} \delta_l$$

where  $c_1$  is a constant,  $a_1 < 0$ , and  $b_1 > 0$ . Since  $a_1 < 0$ , the exponential term can be neglected, and we obtain the following linear relationship:

$$\dot{\phi} = -\frac{b_1}{a_1} \delta_l.$$

That shows that the control input  $\delta_l$  evolves in the same manner as  $\dot{\phi}$ . Thus constraining  $\dot{\phi}$  to be null at the start and at the end of the trajectory will avoid too sharp control input. Using (7) we deduce that  $\ddot{Y} = a_5 a_3 \dot{\phi}$  and finally this constraint deals with  $\ddot{Y}$ . We thus consider the following constraints:

$$\ddot{Y}^*(t_0) = 0, \quad \ddot{Y}^*(t_f) = 0. \quad (9)$$

Taking into account the airplane dynamics as above gives us 8 conditions ((3), (5), (8) and (9)) that  $Y^*(t)$  has to fulfil. That is why we have chosen to determine  $Y^*(t)$  as a 7th-order polynomial:

$$Y^*(t) = at^7 + bt^6 + ct^5 + dt^4 + et^3 + ft^2 + gt + h \quad (10)$$

where the coefficients  $a, b, c, d, e, f, g, h$  are determined so that the 8 conditions (3), (5), (8) and (9) are satisfied. Then a desired "trajectory" can also be determined for roll and heading angles, by using (4) and (7):

$$\psi^*(t) = \frac{1}{a_5} (7at^6 + 6bt^5 + 5ct^4 + 4dt^3 + 3et^2 + 2ft + g) \quad (11)$$

$$\phi^*(t) = \frac{1}{a_3 a_5} (42at^5 + 30bt^4 + 20ct^3 + 12dt^2 + 6et + 2f) \quad (12)$$

In practice, the coefficients  $a, \dots, h$  depend on the initial conditions  $Y_i, \psi_i, \phi_i$ . The duration of the trajectory  $t_f - t_0$  is also chosen as a function of the initial conditions. Indeed it will take more time to align the aircraft with the runway if the lateral error  $Y_i$  is large, and if the heading angle is unfavorable. For example, if  $Y_i < 0$ , an heading angle  $\psi_i > 0$  is a favorable situation (as shown in Fig. 3), whereas  $\psi_i < 0$  is unfavorable (see Fig. 4). In practice, we have used

$$t_f - t_0 = k |Y_i + D \tan(\psi_i)| \quad (13)$$

where  $D$  and  $k$  are fixed once and for all so that the obtained trajectories are feasible (see Section V).

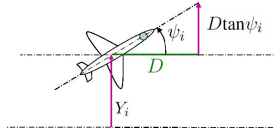


Fig. 4. Initial unfavorable lateral position of the airplane.

2) *Longitudinal Motion*: Using the same approach as before, we consider that the airplane has an initial position  $X_i, Z_i$ , and that its initial velocity and slope are respectively  $v_{a_i}$  and  $\gamma_i$  (see Fig. 5).

The aim is to join the glide path  $Z(X) = X \tan(-\gamma_0)$ , and reach the desired velocity value ( $v_a = v_{a_0}$ ) and slope angle ( $\gamma = \gamma_0$ ).

In order to improve the airplane behaviour when the longitudinal position error is large, a trajectory from initial to desired position is designed. The problem is thus to design a function  $Z^*(X)$  that describes the airplane longitudinal trajectory and enables to reach the glide path from the initial position.

We have considered four conditions that  $Z^*(X)$  must fulfill: the initial position and slope (14), (15), and the final ones (16), (17).

$$Z^*(X_i) = Z_i \quad (14)$$

$$\frac{\partial Z^*}{\partial X}(X_i) = \tan(-\gamma_i) \quad (15)$$

$$Z^*(X_f) = Z_f = X_f \tan(-\gamma_0) \quad (16)$$

$$\frac{\partial Z^*}{\partial X}(X_f) = \tan(-\gamma_0) \quad (17)$$

Then we have determined  $Z^*(X(t))$  as a 3rd-order polynomial:

$$Z^*(X(t)) = aX(t)^3 + bX(t)^2 + cX(t) + d \quad (18)$$

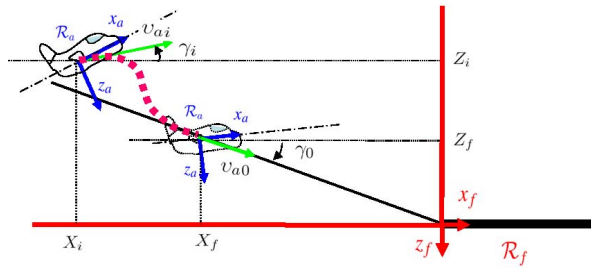


Fig. 5. Airplane longitudinal trajectory to reach glide path.

where the coefficients  $a, b, c, d$  are determined so that the 4 conditions (14), (15), (16) and (17) are satisfied. In practice, they depend to the initial conditions and to the distance  $X_f - X_i$  used to reach the desired path.

### B. Following the Glide Slope

During this phase the airplane has to stay aligned with respect to the runway axis, that is to keep constant the lateral position, roll and heading angles:

$$Y^*(t) = 0, \quad \phi^*(t) = 0, \quad \psi^*(t) = 0. \quad (19)$$

Concerning the longitudinal motion, we keep constant the velocity value and its direction:  $v_a^*(t) = v_{a0}$ ,  $\gamma^*(t) = \gamma_0$ . The desired positions can then be deduced:

$$X^*(t) = \cos(\gamma_0)v_0 dt + X^*(t - dt) \quad (20)$$

$$Z^*(t) = X^*(t)\tan(-\gamma_0) \quad (21)$$

where  $dt$  is the sampling time.

As for the desired pitch angle  $\theta^*(t)$ , we define its variation proportional to the altitude error (following [9], and even if a more complex expression is used in [9]):

$$\theta^*(t) = k(Z(t) - Z^*(t)) + \theta_p \quad (22)$$

where  $k$  and  $\theta_p$  are constant.

### C. Flare and Touchdown

The last phase before touchdown is the flare manoeuvre. It is necessary to round the trajectory, in order to reach suitable vertical velocity and slope when the wheels touch the runway (see Fig. 6).

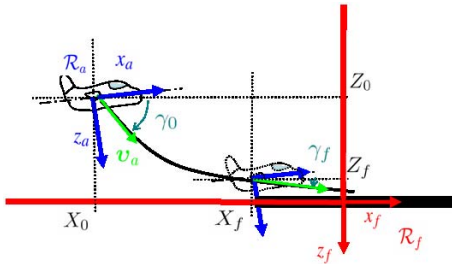


Fig. 6. Airplane longitudinal trajectory during flare.

We have used the following trajectory and vertical velocity profiles [9]:

$$Z^*(X(t)) = \frac{Z_0}{Z_f - Z_0} \left( \dot{Z}_f - \dot{Z}_0 e^{-(X(t) - X_0)/\tau} \right) \quad (23)$$

$$\dot{Z}^*(X(t)) = \dot{Z}_0 e^{-(X(t) - X_0)/\tau} \quad (24)$$

with  $\tau = \frac{Z_0 \dot{X}}{Z_f - Z_0}$ . This choice ensures continuity with the initial position and velocity (25), and final suitable conditions (26).

$$Z^*(X_0) = Z_0, \quad \dot{Z}^*(X_0) = \dot{Z}_0 \quad (25)$$

$$Z^*(X_f) = Z_f = 0, \quad \dot{Z}^*(X_f) = \dot{Z}_f. \quad (26)$$

Since the vertical component of the velocity is reduced, the slope angle is varying. We have used:

$$\gamma^*(t) = -\text{atan} \frac{\dot{Z}^*(t)}{\dot{X}} \quad (27)$$

and the same strategy as previously is used to determine  $\theta^*(t)$  (22).

## IV. VISUAL SERVOING

A camera is fixed on the front of the airplane, and provides images of the runway. Visual features based on the measurements that could be extracted from the image of a runway are considered: they are its two border lines and its central line. In this paper, we do not deal with the image processing but consider that this preliminary step is done (by using [13] for example).

Each runway line projects as a straight line in the image plane, which is represented by the  $(\rho, \theta)$  parameters such that  $x \cos \theta + y \sin \theta - \rho = 0$  (see Fig. 7). These three lines are parallel in the 3D space, but due to the perspective projection model they intersect in the image plane at the vanishing point with coordinates  $x_f$  and  $y_f$ .

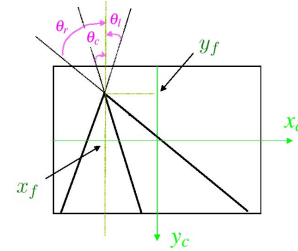


Fig. 7.  $\theta$  parameters and vanishing point.

In [2], we have proposed a control scheme using visual features to follow a runway at specified altitude, velocity and attitude. In this paper, we use the same low-level control, but the desired visual features are obtained from the trajectories presented in the previous section.

To compute the desired image, the three runway lines are projected on the image plane according to the perspective projection model, and using at each iteration the desired airplane position  $(X^*(t), Y^*(t), Z^*(t))$  and orientation  $(\phi^*(t), \theta^*(t), \psi^*(t))$  (given as explained in the previous section). Then the desired visual features  $\theta_c^*(t), \theta_r^*(t), \theta_l^*(t)$  and  $x_f^*(t), y_f^*(t)$  are computed and used in similar control laws as in [2].

We use the following lateral control law:

$$\begin{aligned} \delta_l &= n_1 a_5 (\dot{x}_f - \dot{x}_f^*) + n_2 a_5 (x_f - x_f^*) \\ &+ n_3 \left( Z \frac{\theta_l + \theta_r - 2\theta_c}{c^2 \theta_l^* + c^2 \theta_r^* - 2} - Z^* \frac{\theta_l^* + \theta_r^* - 2\theta_c^*}{c^2 \theta_l^{*2} + c^2 \theta_r^{*2} - 2} \right) \end{aligned} \quad (28)$$

where  $n_1, n_2, n_3$  are chosen so that the system is stable in absence of crosswind [2], and where  $c^2\theta = (\cos\theta)^2$ . As for the longitudinal control law we use:

$$\begin{bmatrix} \tilde{\delta}_m \\ \tilde{\delta}_T \end{bmatrix} = - \begin{bmatrix} \mathbf{K}_m \\ \mathbf{K}_T \end{bmatrix} \begin{bmatrix} y_f - y_f^* \\ \dot{y}_f - \dot{y}_f^* \\ \gamma - \gamma^* \\ v_a - v_a^* \\ \dot{v}_a - \dot{v}_a^* \\ Z - Z^* \end{bmatrix} \quad (29)$$

where the gains  $\mathbf{K}_m, \mathbf{K}_T$  are obtained using a Linear Quadratic Regulator synthesis technique [2].

## V. RESULTS

### A. Experimental Conditions

The proposed trajectory design and control scheme have been tested in a simulation software based on a library provided by the French company Dassault Aviation. This library allows to simulate the behaviour of an airplane equipped with a fly-by-wire control system. It can be controlled by the throttle and the control stick, and it provides pose and state measures.

In order to visualize the world where the airplane is flying around, a visualizer is linked to the library. It allows to place a camera in the 3D environment (for example on the airplane), and visualize the corresponding images (see Fig. 8).

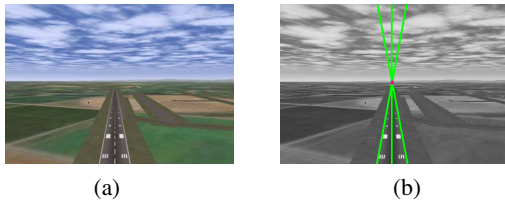


Fig. 8. (a) Runway image from embedded camera. (b) Lines and vanishing point.

The linearized model of the airplane is the one presented in Section II-C. It has been used with the *Control System Toolbox* and the *Matlab/Simulink* tools to design the feedback gains  $\mathbf{K}_m$  and  $\mathbf{K}_T$ .

In order to test the presented control scheme, a feasible glide-path is considered. The aim is to join and follow this glide-path from an initial position, and realize the flare manoeuvre in order to touchdown, using the visual servoing scheme presented in Section IV, and the trajectories presented in Section III.

### B. Results

The aircraft lateral position is initially  $Y = -150$  m (Fig. 11.b) whereas the runway takes place at  $Y_0 = 0$  m. The initial heading is  $\psi_i = -3$  deg (Fig. 11.f) whereas the runway heading is  $\psi_0 = 0$  deg (see Fig. 3). This initial situation is unfavorable, since the airplane has the tendency to move away from the runway axis ( $\psi_i < 0$ , see Fig. 4). Despite this unfavorable situation, the proposed lateral control scheme enables to align with the runway in about 50 seconds. Concerning the duration of the desired

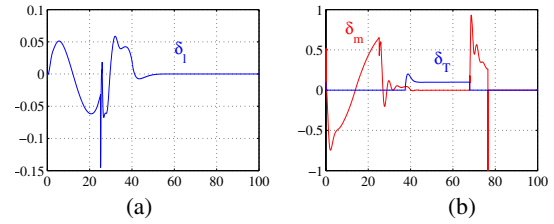


Fig. 9. Time evolution (in seconds) of the control inputs: lateral position of the control stick  $\delta_l$  (a), and longitudinal position of the control stick  $\delta_m$  and throttle position  $\delta_T$  (b).

trajectory (13), we have chosen  $D = 40$  and  $k = 0.26$ , that leads to  $t_f - t_0 \simeq 40$  s. We can see on Fig. 10 that the desired trajectory  $Y^*(t)$ , in the  $XY$  plane, takes into account the initial tendency to move away from the runway axis, and shows smooth initial and final transitions. We can see on Fig. 11.b that the desired lateral position  $Y^*(t)$  is easily followed, despite a small overshoot and a little delay. Using the airplane model to design the heading and roll desired values strongly improve the behaviour of the airplane, because the values to be reached are feasible. The current values follow quite well the desired ones (see Fig. 11.d and 11.f). The small differences can be explained by the fact that the linearized model used is only an approximation of the airplane dynamics. The visual features introduce also small perturbations, since we have neglected some coupling [2]. The control input  $\delta_l$  (left-right position of the control stick) is smooth at the start and at the end of the trajectory, as expected (Fig. 9.a). The transient perturbation at  $t \simeq 25$  s is induced by the longitudinal behaviour. It can be seen on Fig. 13 that the error on the visual data used in the lateral control law (28) remains quite small and that they converge to the desired values.

As for the longitudinal motion, the desired glide-slope is defined by the airspeed  $v_{a0} = 55.28$  m/s, and the slope angle  $\gamma_0 = -5.5$  deg (Fig. 5). Since the initial distance between the aircraft and the runway is  $X = -4100$  m (Fig. 11.a), its initial altitude should be  $Z = -4100 \tan(5.5) \simeq -394$  m. But the initial altitude is  $Z_i = -490$  m (Fig. 11.c). The longitudinal trajectory (Fig. 10) enables to reach the desired glide path: the velocity and slope angle reach their desired values at  $t \simeq 40$  s (see Fig. 12). The throttle input and the backward-forward position of the control stick are used to realize correctly this task, and at the end they reach their equilibrium values too (see Fig. 9.b).

Then (between  $t = 50$  s and  $t = 68$  s), the airplane follows the desired glide path, the parameters are approximately constant.

When  $Z = -20$  m, the flare manoeuvre is initiated, in order to elevate the nose of the airplane (Fig. 11.e), to round the trajectory (see Fig. 10 and 12.b) and to decrease the vertical velocity. After touchdown, the airplane velocity is driven to 0.

## VI. CONCLUSION

In this paper, a visual servoing scheme allowing an airplane to land automatically has been proposed. A trajectory design using the airplane model enables to deal with large initial error and to reach the desired glide path. The control

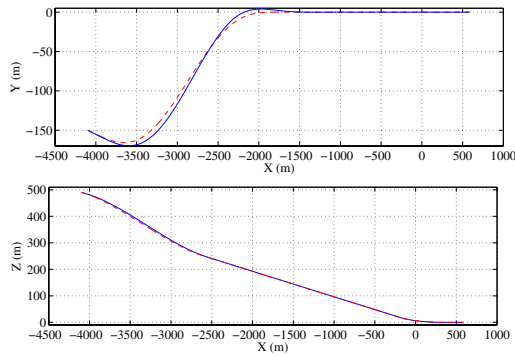


Fig. 10. Lateral trajectory  $Y(X(t))$  in the horizontal plane (a) and longitudinal trajectory  $Z(X(t))$  in the vertical plane (b). The dashed red line is the desired trajectory and the blue line is the current one.

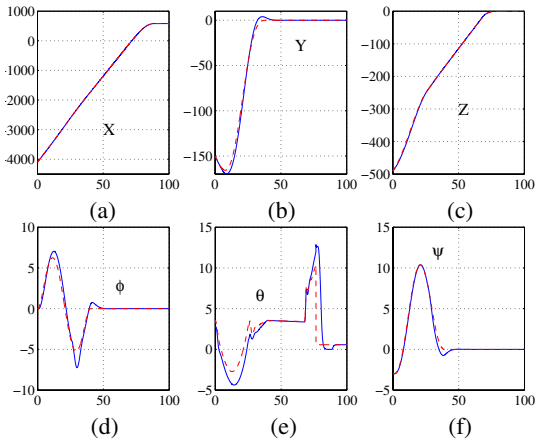


Fig. 11. Time evolution (in seconds) of the position (m) and attitude (deg) of the airplane. The desired values are plotted in red, and the current ones in blue.

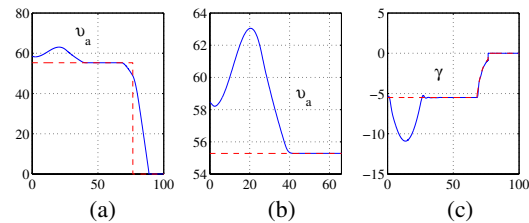


Fig. 12. Time evolution (in seconds) of the velocity  $v_a$  (m/s) (a and b), and slope  $\gamma$  (c). The desired values are plotted in red, and the current ones in blue.

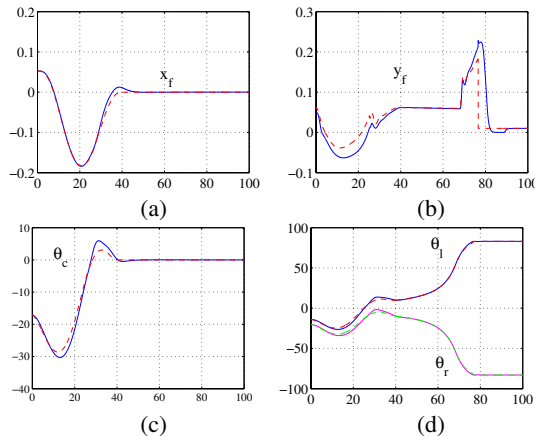


Fig. 13. Time evolution (in seconds) of the visual features: coordinates of the vanishing point:  $x_f$  (a) and  $y_f$  (b) (m), and  $\theta_l$  (c),  $\theta_r$  and  $\theta_c$  (d) (deg). The desired values are plotted in red, and the current ones in blue.

scheme uses a linearized model of the airplane dynamics and decoupled visual features. Simulation results show that the proposed scheme enables the airplane to realize the entire auto-landing task, from approach mode to flare manoeuvre and touch-down.

## VII. ACKNOWLEDGMENTS

This work has been supported by a DGA grant. The authors strongly thank Bruno Patin, Jean-Pierre Belmont, Jean-Pierre Tomaszower, Guillaume Rimbault and Erica Palmyre from Dassault Aviation for providing the flight simulator, the dynamical airplane model and for useful discussions.

## REFERENCES

- [1] J. R. Azinheira, P. Rives, J. R. H. Carvalho, G. F. Silveira, E. C. de Paiva, and S. S. Bueno, *Visual Servo Control for the Hovering of an Outdoor Robotic Airship*, ICRA'02, pp. 2787-2792, Vol. 3, Washington, USA, May 2002.
- [2] O. Bourquardez and F. Chaumette, *Visual Servoing of an Airplane for Alignment with respect to a Runway*, ICRA'07, pp. 1330-1335, Roma, Italia, April 2007.
- [3] E. D. Dickmanns, and F. R. Schell, *Autonomous landing of airplanes by dynamic machine vision*, IEEE Workshop on Applications of Computer Vision, Palm Springs, CA, USA.
- [4] B. Espiau, F. Chaumette, and P. Rives, *A new approach to visual servoing in robotics*, ITRA, 8(3):313-326, 1992.
- [5] E. Frew, T. McGee, Z. Kim, X. Xiao, S. Jackson, M. Morimoto, S. Rathinam, J. Padial, R. Sengupta, *Vision-Based Road Following Using a Small Autonomous Aircraft*, IEEE Aerospace Conference, Big Sky, MT, March 2004.
- [6] J. Gangloff, M. de Mathelin, *High speed visual servoing of a 6 DOF manipulator using MIMO predictive control*, ICRA'00, pp. 3751-3756, Vol.4, San Francisco, CA, USA, April 2000.
- [7] S. Hutchinson, G. Hager, P. I. Corke, *A tutorial on visual servo control*, ITRA, Vol.12, No. 5, pp. 651-670, 1996.
- [8] H. Izadi, M. Pakmehr, and N. Sadati, *Optimal neuro-controller in longitudinal auto-landing of a commercial jet transport*, IEEE Conference on Control Applications, pp. 492-497, vol.1, June 2003.
- [9] C. C. Jorgensen and C. Schley, *A neural network baseline problem for control of aircraft flare and touchdown*, Neural networks for control, 1990, pp. 403-425, MIT Press, Cambridge, MA, USA.
- [10] Y. Li, Z. Wang, N. Sundararajan, P. Saratchandran, *Neuro-controllers for aircraft auto-landing under severe wind conditions*, ACC, pp. 1296- 1301, vol. 2, June 2003.
- [11] R. Mahony, T. Hamel, *Image-based visual servo control of aerial robotic systems using linear image features*, ITRA'05, pp. 227- 239, Vol.21, April 2005.
- [12] E. Malis, F. Chaumette, S. Boudet, *2 1/2 D visual servoing*, ITRA, Vol.15(2), pp. 238-250, April 1999.
- [13] E. Marchand, P. Bouthemy, F. Chaumette, and V. Moreau, *Robust Real-Time Visual Tracking Using a 2D-3D Model-Based Approach*, ICCV, Corfu, Greece, 1999.
- [14] L. Mejias, S. Saripalli, G. Sukhatme, P. Campoy, *Detection and tracking of external features in a urban environment using an autonomous helicopter*, ICRA'05, pp. 3983-3988, Barcelone, Espagne, April 2005.
- [15] P. Rives, J. R. Azinheira, *Visual Auto-landing of an Autonomous Aircraft*, Research Report INRIA-Sophia Antipolis, No 4606, November 2002.
- [16] P. Rives, J. R. Azinheira, *Linear Structures Following by an Airship using Vanishing Point and Horizon Line in Visual Servoing Scheme*, ICRA'04, pp. 255-260, Vol.1, New Orleans, April 2004.
- [17] S. Saripalli, J. F. Montgomery, G. S. Sukhatme, *Visually-guided landing of an unmanned aerial vehicle*, ITRA, Vol. 19, No. 3, pp. 371-381, June 2003.
- [18] C. S. Sharp, O. Shakernia, S. S. Sastry, *A vision system for landing an unmanned aerial vehicle*, ICRA'01, pp. 1720 - 1727, Vol.2, Seoul, Korea, May 2001.
- [19] G. F. Silveira, J. R. Azinheira, P. Rives, S. S. Bueno, *Line Following Visual Servoing for Aerial Robots Combined with Complementary Sensors*, ICAR, Coimbra, Portugal, pp. 1160-1165, July 2003.
- [20] H. Zhang, J. P. Ostrowski, *Visual servoing with dynamics: Control of an unmanned blimp*, ICRA'99, pp. 618-623, Vol.1, Detroit, USA, May 1999.